Journal of Software Engineering

ISSN 1819-4311

Academic Journals Inc.

www.academicjournals.com

Journal of Software Engineering 9 (3): 548-560, 2015
ISSN 1819-4311 / DOI: 10.3923/jse.2015.548.560

The Analysis and Implementation of Proportional Resonant Control Algorithm-based Pwm Inverter Imbalanced Grid-connected

Zhang Jun-Li, Li Yu-Ren, Wang Peng, Liang Bo and FU Long-Fei
School of Automatic Control, Northwestern Polytechnical University, Xi'an, 710072, China

Corresponding Author: Zhang Jun-li, School of Automatic Control, Northwestern Polytechnical University, Xi'an, 710072, China

ABSTRACT

The mathematical model of Pulse Width Modulation (PWM) inverter was established. According to the symmetrical components theory, the phenomena of 2nd ripple in the DC side voltage of PWM inverter fed by imbalanced grid voltage was analyzed. The control performance degradation of traditional control methods was caused by the presence of negative sequence components. The Proportional Resonant (PR) control algorithm was proposed in detail in this paper. The improved PR control algorithm was applied to control PWM inverter fed by imbalanced grid voltage. The improved PR controller could effectively reduce the 2nd ripple in PWM inverter DC side voltage and could reduce harmonic content of PWM inverter AC side current. Thereby the PR controller proposed could improve the control performance of the PWM inverter. The effectiveness of the proportional resonant control algorithm proposed was demonstrated by the simulation results in MATLAB.

Key words: Inverter, imbalanced grid voltage, ripple, symmetrical components theory, proportional resonant control

INTRODUCTION

Due to many advantages such as sinusoidal input current, power factor being controlled, smaller capacitors in dc side achieving high quality output voltage, active power and reactive power flowing bi-directional and being adjusted independently, etc., three-phase PWM inverter grid-connected has been widely employed in a few of fields of motor four-quadrant operation, new energy generation systems, flexible AC transmission system and other industrial domains (Fujita *et al*., 1993; Jung *et al*., 1996; Malesani *et al*., 1996; Shiraishi *et al*., 2004; Suh and Lipo, 2004).

Zhan *et al*. (2005) investigated QRDCL soft-switching 3-dimensional hysteresis current control for power quality compensator and the easy time sequence matching simplifies the system control. De Paula *et al*. (2005) presented a time domain methodology for cable modeling able to represent the cable parameters variation due to skin effect in this broad range of frequencies. It included frequency-dependent cable earth-return model, allowing the computation of the zero-sequence currents generated by the common-mode voltage produced by the inverter. Mihalache (2005) detailed the multi-loop method, positive and negative sequence controllers were used to regulate the fundamental currents and resonant controllers tuned to each harmonic from third to thirteenth remove the low frequency components. Oshikata *et al*. (2007) proposed the suitable switching sequence for partial resonance and it was required to achieve full ZVS on the main switches after

partial resonance. De Paula *et al.* (2008) proposed a time domain methodology for cable modeling, which could reproduce accurately the wave propagation and reflection phenomena, thus showing to be very appropriate to transient overvoltage studies in PWM motor drives. It included a new alternative to represent the frequency-dependent cable earth-return path. Borage *et al.* (2009) studied the characteristics of an ADC controlled LCL-T resonant converter operating at the resonant frequency. In four operating modes, different conditions during the device switching was created. The mode boundaries are obtained and plotted on the D-Q plane. A region on the D-Q plane is identified for the converter design. Hsu and Chao (2009) discussed the trend in ac adapters for notebook computers which aims to offer smaller size, higher efficiency and lower price along with a highly integrated BCM PFC and QR PWM combo controller. A built-in THD optimizer improved THD at light load and the controller rapidly protected this cycle-by-cycle sampling in case of output over voltage.

Nouri and Ghasemzadeh (2011) proposed a FDG with a new control scheme for the purpose of contributing to power generation and harmonic compensation under non-ideal source voltages. The proportional resonant controllers were used for reference signal tracking. Cetin and Hava (2012) investigated the CMV/CMC properties of the two and three-level VSIs for various PWM methods and it provided a comprehensive leakage current evaluation. Chen *et al.* (2013) presented a dual power control scheme to control the active and reactive power independently under the unbalanced power grid voltage conditions. Chen *et al.* (2013), the proportional resonant controller was in the outer loop suppresses the DC-link ripple and the PI repetitive control was applied in the inner loop to eliminate active and reactive power oscillation. Yang *et al.* (2013) proposed an easy method to design the PR regulator parameters separately, which can guarantee the stability of the system and the performance of the inner current loop. Russi *et al.* (2013) provided a mathematical expression to determine the occurrence of soft-switching for a general topology of ZVT converters with auxiliary resonant voltage source. The proposed conditions was useful for analysis and design, allowing evaluating operation sequence, total commutation time, resistive losses and other important parameters to describe the converter performance. Xu *et al.* (2013) proposed a novel compensation system consisting of a three-phase three windings V/v transformer, passive filters and a three-phase VSC. Xu *et al.* (2013), the harmonic suppression theory, the negative sequence current compensation principle, a novel reference current detection algorithm and the quasi proportional resonance were presented.

In this study, the mathematical model of PWM inverter fed by imbalanced grid voltage was established. According to the analysis via symmetrical components theory, there was 2nd ripple content in the DC side voltage and plenty of harmonic content in the AC side currents of PWM inverter. The proportional resonant control strategy was described in this study and a more in-depth study was conducted in it. The PR control strategy was applied to control PWM inverter fed by imbalanced grid voltage. The method of adjusting its resonant frequency to two times of the fundamental frequency could effectively reduce the harmonic content in PWM inverter DC side voltage. Compared with the traditional control methods, the control method proposed in this study could effectively reduce the harmonic content of PWM inverter while it did not affect the dynamic response of PWM inverter. The control method proposed could improve the power factor of the inverter and it could be extended to the relevant applications of the inverter.

METHODOLOGY

Mathematical model of the PWM inverter grid-connected: The schematic diagram of the voltage source PWM inverter is shown Fig. 1 (Shiraishi *et al.*, 2004; Suh and Lipo, 2004;

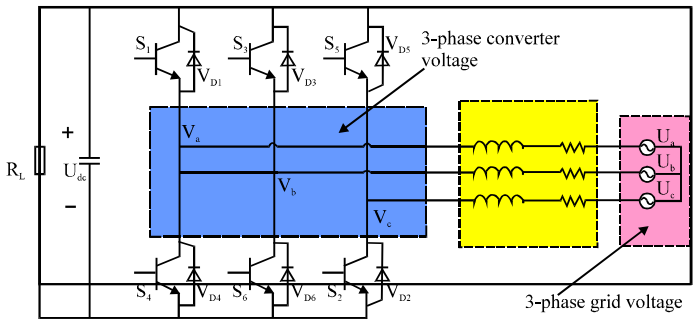

Fig. 1: Schematic of grid-connected PWM inverter

Mihalache, 2005). In Fig. 1, u_a, u_b and u_c is the instantaneous voltage value of a, b, c-phase of the grid, respectively, v_a, v_b and v_c is the instantaneous voltage value of a, b, c-phase of the inverter ac side, respectively, i_a, i_b and i_c is the instantaneous current value of a-phase, b-phase, c-phase of the grid respectively, L is the inductance value of line reactor, R is the line resistance, C is the capacitance of the dc side and u_{dc} is its both ends voltage, R_L is the load resistance. According to Kirchhoff's voltage theorem, the voltage equation of voltage source PWM inverter in three-phase stationary coordinate can be obtained as Eq. 1:

$$\frac{d}{dt}\begin{bmatrix} i_a \\ i_b \\ i_c \end{bmatrix} + \frac{R}{L}\begin{bmatrix} i_a \\ i_b \\ i_c \end{bmatrix} + \frac{1}{L}\begin{bmatrix} i_a \\ i_b \\ i_c \end{bmatrix} - \frac{1}{L}\begin{bmatrix} u_a - v_a \\ u_b - v_a \\ u_c - v_a \end{bmatrix} = 0 \tag{1}$$

The change rates of active and reactive power in $\alpha\beta$ coordinates can be given in Eq. 2:

$$\begin{aligned} &\frac{d}{dt}\begin{bmatrix} p \\ q \end{bmatrix} + \frac{d}{dt}\begin{bmatrix} u_\alpha & u_\beta \\ u_\beta & u_\alpha \end{bmatrix} \bullet \begin{bmatrix} i_\alpha \\ i_\beta \end{bmatrix} + \begin{bmatrix} u_\alpha & u_\beta \\ u_\beta & -u_\alpha \end{bmatrix} \bullet \frac{d}{dt}\begin{bmatrix} i_\alpha \\ i_\beta \end{bmatrix} \\ &= \begin{bmatrix} \frac{du_\alpha}{dt} & \frac{du_\beta}{dt} & u_\alpha & u_\beta \\ \frac{du_\beta}{dt} & \frac{du_\alpha}{dt} & u_\beta & -u_\alpha \end{bmatrix} \begin{bmatrix} i_\alpha \\ i_\beta \\ \frac{di_\alpha}{dt} \\ \frac{di_\beta}{dt} \end{bmatrix} \end{aligned} \tag{2}$$

The Eq. 3 can be described as:

$$\frac{d}{dt}\begin{bmatrix} p \\ q \end{bmatrix} = -\frac{1}{L}\begin{bmatrix} R \cdot p \\ R \cdot q \end{bmatrix} + \begin{bmatrix} -\omega q \\ \omega p \end{bmatrix} + \frac{1}{L}\begin{bmatrix} (u_\alpha^2 + u_\beta^2) - (u_\alpha \cdot u_\beta + v_\alpha \cdot v_\beta) \\ u_\alpha \cdot u_\beta - v_\alpha \cdot v_\beta) \end{bmatrix} \tag{3}$$

The distribution of inverter voltage vectors and its sectors are shown in Fig. 2 (De Paula *et al.*, 2008; Soltanzadeh *et al.*, 2014). There are six active voltage vectors and two zero voltage vectors in Fig. 2 and the subscript of the voltage vector represents the switching mode of phase a, b and

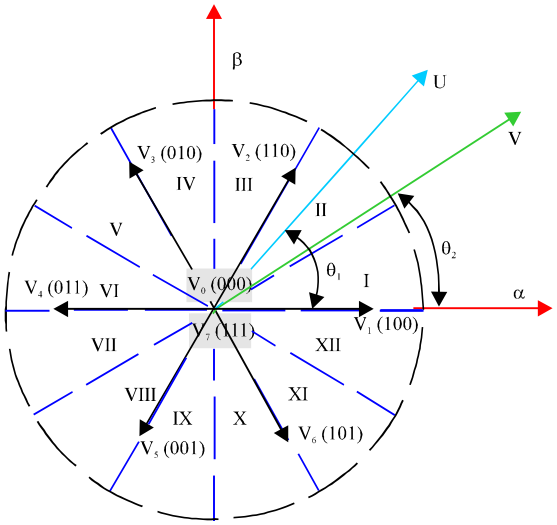

Fig. 2: Distribution of inverter voltage vectors and its sectors

Table 1: Switching states and voltage vectors of inverter

I	Sc Sb Sa	Vi
0	0 0 0	$V_0 = 0$
1	0 0 1	$V_1 = \frac{2}{3}u_{dc}\angle 0 = \frac{2}{3}u_{dc}$
2	0 1 1	$V_2 = \frac{2}{3}u_{dc}\angle\frac{1}{3}\pi = \frac{1}{3}u_{dc} + j\frac{\sqrt{3}}{3}u_{dc}$
3	0 1 0	$V_3 = \frac{2}{3}u_{dc}\angle\frac{2}{3}\pi = \frac{1}{3}u_{dc} + j\frac{\sqrt{3}}{3}u_{dc}$
4	1 1 0	$V_4 = \frac{2}{3}u_{dc}\angle\pi = -\frac{2}{3}u_{dc}$
5	1 0 0	$V_5 = \frac{2}{3}u_{dc}\angle -\frac{2}{3}\pi = -\frac{1}{3}u_{dc} - j\frac{\sqrt{3}}{3}u_{dc}$
6	1 0 1	$V_6 = \frac{2}{3}u_{dc}\angle -\frac{1}{3}\pi = \frac{1}{3}u_{dc} - j\frac{\sqrt{3}}{3}u_{dc}$
7	1 1 1	$V_7 = 0$

c, respectively. The switching states and the corresponding voltage vector values of PWM inverter grid-connected in two-phase stationary **αβ** coordinate are shown in Table 1, where S_a, S_b and S_c represents the switching status of phase a, b, c, respectively and $S_k = 1$ represents the upper switch in phase k turning on and the under switch turning off, $S_k = 0$ denotes the upper switch in phase k turning off and the under switch turning on, where k = a, b, c; V_i indicates the inverter voltage vector in i_{th} sector, where i = I, II,..., XII.

When the three-phase grid voltage is imbalanced, there are positive sequence component, negative sequence components and zero sequence components in the electrical variables of the PWM inverter fed by the grid according to the symmetrical components theory (Pan *et al*., 2014; Xu *et al*., 2014; Zeng *et al*., 2014). For the three-phase three-wire PWM inverter fed by the grid, there is no zero sequence components without neutral wire. Only the positive sequence component and negative sequence component were considered. Coordinate transformation relationship between the electrical variables was shown in Eq. 4:

$$\begin{cases} F_{\alpha\beta} = F_{dq}^{p} e^{j\omega t} \\ F_{\alpha\beta} = F_{dq}^{n} e^{-j\omega t} \\ F_{dq}^{p} = F_{dq}^{n} e^{-j\omega t} \\ F_{dq}^{n} = F_{dq}^{p} e^{j2\omega t} \end{cases} \tag{4}$$

The three-phase grid voltages could be decomposed into positive and negative sequence preamble section, as Eq. 5:

$$\begin{cases} F_{\alpha\beta} = E_{\alpha\beta}^{p} + E_{\alpha\beta}^{n} = E_{dq+}^{p} e^{j\omega t} + E_{dq-}^{n} e^{-j\omega t} \\ E_{dq+}^{p} = E_{d+}^{p} + jE_{d+}^{p} \\ E_{dq-}^{p} = F_{d-}^{n} + jE_{q-}^{n} \\ E_{\alpha\beta} = \dfrac{2}{3}\left(E_a + E_b e^{j\frac{2\pi}{3}} + E_c e^{-j\frac{2\pi}{3}} \right) \end{cases} \tag{5}$$

In Eq. 5, ω is the angular frequency of the grid voltage. The superscripts p and n denote positive sequence component and negative sequence component respectively. The subscript + and - denote positive and negative synchronous rotating coordinate system, respectively. The variables in negative sequence synchronous rotating coordinate system was transformed into the ones in the positive synchronous rotating coordinate system as shown in Eq. 6:

$$E_{dq+} = E_{dq+}^{p} + E_{dq+}^{n} = E_{dq+}^{p} + E_{dq-}^{n} e^{-j2\omega t} \tag{6}$$

In Eq. 6, It could be seen that in the condition of imbalanced grid voltage, the grid voltage was transformed into the synchronous rotating coordinate system. The grid voltage included the positive sequence DC component and negative sequence two times fundamental frequency harmonic fluctuations AC component:

$$\begin{cases} U_{\alpha\beta} = RI_{\alpha\beta} + L\dfrac{dI_{\alpha\beta}}{dt} + E_{\alpha\beta} \\ U_{\alpha\beta} = \dfrac{2}{3}\left(U_a + U_b e^{j\frac{2\pi}{3}} + U_c e^{-j\frac{2\pi}{3}} \right) = E_{dq+}^{p} e^{j\omega t} + E_{dq-}^{n} e^{-j\omega t} \\ I_{\alpha\beta} = \dfrac{2}{3}\left(I_a + I_b e^{j\frac{2\pi}{3}} + I_c e^{-j\frac{2\pi}{3}} \right) = I_{dq+}^{p} e^{j\omega t} + I_{dq-}^{n} e^{-j\omega t} \end{cases} \tag{7}$$

As can be seen from Eq. 7, when the grid voltage was imbalance, the positive sequence component and the negative sequence component in synchronous rotating coordinate system of the PWM inverter fed by the grid were given in Eq. 8:

$$\begin{cases} U_{dq+}^{p} = RI_{dq+}^{p} + L\dfrac{dI_{dq+}^{p}}{dt} + j\omega LI_{dq+}^{p} + E_{dq+}^{p} \\ U_{dq-}^{n} = RI_{dq-}^{n} + L\dfrac{dI_{dq-}^{n}}{dt} + j\omega LI_{dq-}^{n} + E_{dq-}^{n} \end{cases} \tag{8}$$

The complex power, active power and reactive power of the PWM inverter fed by the grid were given in Eq. 9:

$$\begin{cases} S = P + jQ = \frac{2}{3} EI^* = \frac{2}{3}\left(E^p_{dq+} e^{j\omega t} + E^n_{dq-} e^{-j\omega t}\right)\left(I^p_{dq+} e^{j\omega t} + I^n_{dq-} e^{-j\omega t}\right)^* \\ P = P_0 + P_{c2}\cos(2\omega t) + P_{s2}\sin(2\omega t) \\ Q = Q_0 + Q_{c2}\cos(2\omega t) + Q_{s2}\sin(2\omega t) \end{cases} \tag{9}$$

In Eq. 9, P_0 and Q_0, respectively, was the average value of P and Q. P_{c2} and P_{s2}, respectively, was the amplitude of the two times fundamental frequency fluctuation component in P. Q_{c2} and Q_{s2}, respectively, was the amplitude of the two times fundamental frequency fluctuation component in Q. P_0, Q_0, P_{c2}, P_{s2}, Q_{c2} and Q_{s2} were defined in Eq. 10:

$$\begin{cases} P_0 = \frac{2}{3}\left(E^p_{d+}I^p_{d+} + E^p_{q+}I^p_{q+} + E^n_{d-}I^n_{d-} + E^n_{q-}I^n_{q-}\right) \\ P_{c2} = \frac{2}{3}\left(E^n_{d-}I^p_{d+} + E^n_{q-}I^p_{q+} + E^p_{d+}I^n_{d-} + E^p_{q+}I^n_{q-}\right) \\ P_{s2} = \frac{2}{3}\left(E^n_{q-}I^p_{d+} - E^n_{d-}I^p_{q+} - E^p_{q+}I^n_{d-} + E^p_{d+}I^n_{q-}\right) \\ Q_0 = \frac{2}{3}\left(E^p_{q+}I^p_{d+} - E^p_{d+}I^p_{q+} + E^n_{q-}I^n_{d-} - E^n_{d-}I^n_{q-}\right) \\ Q_{c2} = \frac{2}{3}\left(E^n_{q-}I^n_{d+} - E^n_{d-}I^n_{q+} + E^p_{q+}I^n_{d-} - E^p_{d+}I^n_{q-}\right) \\ Q_{s2} = \frac{2}{3}\left(-E^n_{d-}I^p_{d+} - E^n_{q-}I^p_{q+} + E^p_{d+}I^n_{d-} + E^p_{q+}I^n_{q-}\right) \end{cases} \tag{10}$$

Analysis of proportional resonant control algorithm: The zero static error control of the AC input signal could be achieved via Proportional Resonant (PR) controller. The PR controller could be applied to control PWM inverter fed by the grid, could regulate the current in two-phase stationary coordinate system. It could simplify the coordinate transformation of control process, could eliminate the current error in two-phase stationary coordinate system. It could eliminate coupling relationship between the current in d-axis and q-axis component and it could ignore the disturbance role of the grid voltage to the PWM inverter (Karimi *et al*., 2014; Qu and Zhao, 2014).

PR controller: PR controller, namely the proportion of resonant controller, was composted with the proportion section and the resonant section (Pokryszko-Dragan *et al*., 2014; Bai *et al*., 2014). PR controller could achieve no static error control to the sine signal. The transfer function of ideal PR controller was given in Eq. 11:

$$G(s) = K_p + \frac{K_R S}{S^2 + \omega_0^2} \tag{11}$$

where, K_p is the proportional coefficient, K_R is the resonance coefficient, ω_0 is the resonant frequency. The integral section of the PR controller was also known as the generalized integrator, which could integrate the amplitude of the sine signal in the resonant frequency points.

For the input signal with the same frequency Msin(ωt+φ), the response analysis in time domain was as below.

Laplace transform of the input signal was as Eq. 12:

$$\begin{aligned} &L(M\sin(\omega t+\varphi)=L(M\sin(\omega t)\cos\varphi+M\cos\varphi+M\cos(\omega t)\sin\varphi)\\ &=M\cos\varphi*\frac{\omega}{s^2+\omega^2}+M\sin\varphi*\frac{s}{s^2+\omega^2} \end{aligned} \tag{12}$$

After $\frac{K_R S}{S^2+\omega_0^2}$ the expression was as Eq. 13:

$$\begin{aligned} &\left(M\cos\varphi*\frac{\omega}{s^2+\omega^2}+M\sin\varphi*\frac{s}{s^2+\omega^2}\right)*\frac{K_R S}{S^2+\omega_0^2}\\ &=K_R*M*\left(\cos\varphi*\frac{\omega s}{(s^2+\omega^2)^2}+\sin\varphi*\frac{s^2}{(s^2+\omega^2)^2}\right)\\ &=K_R*M*\left(\cos\varphi*\frac{\omega s}{(s^2+\omega^2)^2}+\frac{\sin\varphi}{2}*\left[\frac{s^2-\omega^2}{(s^2+\omega^2)^2}+\frac{1}{s^2+\omega^2}\right]\right) \end{aligned} \tag{13}$$

Laplace transform of tsinωt was in Eq. 14:

$$\begin{aligned} &L(t\sin\omega t)=L\left(\frac{te^{j\omega t}-te^{-j\omega t}}{2j}\right)\\ &=\frac{1}{2j}\left(L(te^{j\omega t})-L(te^{-j\omega t})\right)\\ &=\frac{1}{2j}\left(\frac{1}{(s-j\omega)^2}-\frac{1}{(s+j\omega)^2}\right)\\ &=\left(\frac{4j\omega s}{(s-j\omega)^2(s+j\omega)^2}\right)\\ &=\frac{2\omega s}{(s^2+\omega^2)^2} \end{aligned} \tag{14}$$

Laplace transform of tcosωt was in Eq. 15:

$$\begin{aligned} &L(t\sin\omega t)=L\left(\frac{te^{j\omega t}+te^{-j\omega t}}{2j}\right)\\ &=\frac{1}{2j}\left(L(te^{j\omega t})+L(te^{-j\omega t})\right)\\ &=\frac{1}{2j}\left(\frac{1}{(s-j\omega)^2}+\frac{1}{(s+j\omega)^2}\right)\\ &=\left(\frac{s^2-\omega^2}{(s-j\omega)^2(s+j\omega)^2}\right)\\ &=\frac{s^2-\omega^2}{(s^2+\omega^2)^2} \end{aligned} \tag{15}$$

The anti-Laplace transform of Eq. 13 was as Eq. 16:

$$\begin{aligned} & L^{-1}\left(K_R * M * \left(\cos\varphi * \frac{\omega s}{(s^2+\omega^2)^2} + \frac{\sin\varphi}{2} * \left[\frac{s^2+\omega^2}{(s^2+\omega^2)^2} + \frac{1}{s^2+\omega^2}\right]\right)\right) \\ & = K_R * M * \left(\frac{\cos\varphi}{2} * t\sin(\omega t) + \frac{\sin\varphi}{2} * \left[t\cos(\omega t) + \frac{1}{\omega}\sin(\omega t)\right]\right) \\ & = \frac{K_R * M}{2} * \left(\left(t\cos\varphi + \frac{\sin\varphi}{\omega}\right)\sin(\omega t) + t\sin\varphi * \cos(\omega t)\right) \end{aligned} \tag{16}$$

From the above equation, when $\varphi = 0$, the output signal of the resonant controller was:

$$\frac{K_R * M}{2} * (t\sin(\omega t))$$

which was the same phase with the input signal and the amplitude linear increasing with time.

At that time $\varphi = 90°$, the output signal of the resonance controller was as:

$$\frac{K_R * M}{2} * \left(\frac{1}{\omega}\sin(\omega t) + t\cos(\omega t)\right)$$

When the time was slightly longer, the value close to cos(ωt). From the overall look of the resonator (or so-called generalized integrator), it was by the time increments with the error signal. As shown in Fig. 3, the integral part of PR controller in the resonant frequency point could achieve infinite gain and was with little attenuation in addition to the resonant frequency. Therefore, in order to selectively compensate the harmonic, PR controller could be used as a right-angle filter.

Quasi-PR controller: As shown in section above, compared with PI controller, PR controller could achieve zero steady-state error and selectively improve the ability of anti disturbances from grid

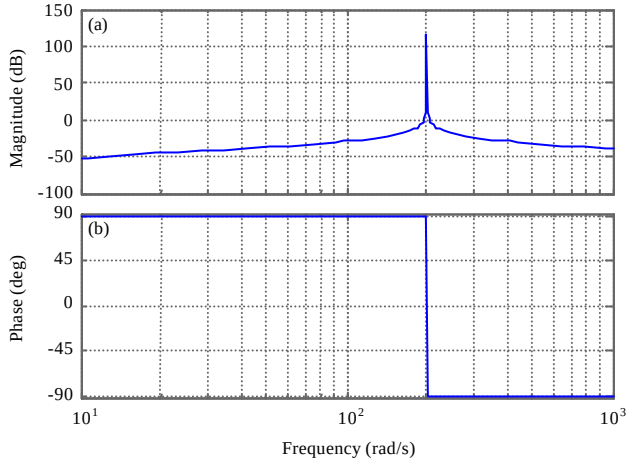

Fig. 3: Bode plot of ideal proportional resonant controller

voltage (Chu *et al*., 2014; Bao *et al*., 2014). But in actual system applications, the achievement of PR controller implied two main problems. The one was that PR controller was not easy to be achieved for the accuracy restriction of the analog system component parameters and digital system and the other was that as PR controller gain at non-fundamental frequency points was very small, it could not effectively suppress harmonics from the grid while an offset in grid frequency.

Therefore, on the basis of PR controller, a quasi-PR controller easy to implement was proposed. The quasi-PR controller could either maintain high gain as PR controller but also could effectively reduce the impact on inverter output inductor current while the grid frequency offset.

The transfer function of Quasi-PR controller was in Eq. 17:

$$G(s) = K_p + \frac{2K_R\omega_c s}{s_2 + 2\omega_c s + \omega_0^2} \tag{17}$$

It could be seen from the Bode plot of PR controller that the amplitude-frequency characteristics of PR controller in the fundamental frequency was $A(\omega_0)$ = 60dB and the margin of phase angle was infinite. Basically, it could achieve zero steady-state error but also had good steady margin and transient performance.

RESULTS

In order to validate the effectiveness of the proposed proportional resonant controller-based PWM inverter at unbalanced grid voltages, simulation results were given in this section. The asymmetric three-phase grid voltage drop was studied, the PWM simulation system parameters were shown in Table 2.

The simulation model of PWM inverter at asymmetric grid voltages was built in MATLAB software and its system characteristics was analyzed. The proposed method of proportional resonant control was compared with conventional control methods. The asymmetric three-phase grid voltages were shown in Fig. 4, in which the voltage amplitude of phase-a is 100 V, that of phase-b is 130 V and that of phase-c is 120 V. When the three-phase PWM inverter was fed with the asymmetric grid given in Fig. 4, its three-phase currents were shown in Fig. 5. It can be seen that the three-phase currents is also asymmetric. In the traditional control methods, the direct axis current or cross-axis current of PWM inverter AC side currents via rotating coordinate transformation was not controlled. There was always the presence of the 2nd ripple in PWM inverter DC side voltage. The proposed proportional resonant control strategy could effectively reduce the 2nd ripple in PWM

Table 2: Circuit parameters of PWM inverter

Parameters	Value
Phase voltage Rms of power supply (Usi/V)	270
Voltage frequency of power supply (f/Hz)	50
Voltage of dc side capacitor (Udc/V)	750
Capacitor in dc side (C/μF)	2000
Reactor Inductance (L/mH)	5
Equivalent resistance (R/Ω)	0.1
Load resistance (RL/Ω)	12
Switching frequency /kHz	5
Sampling frequency /kHz	5
Dead time (Td/μs)	5

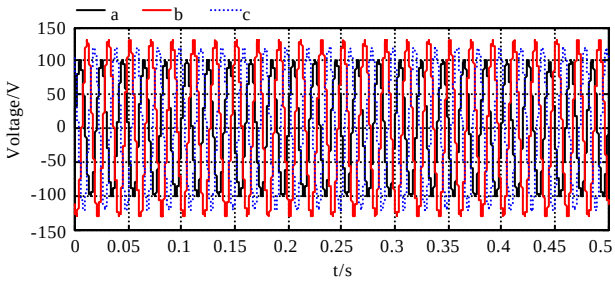

Fig. 4: The imbalanced grid voltages

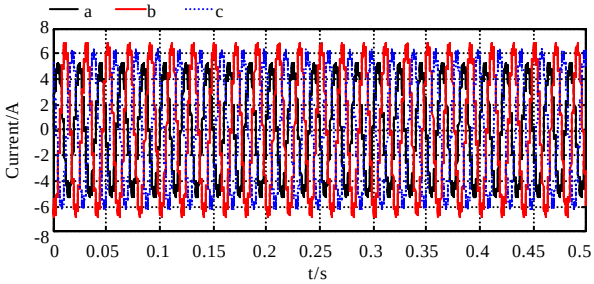

Fig. 5: The imbalanced grid currents

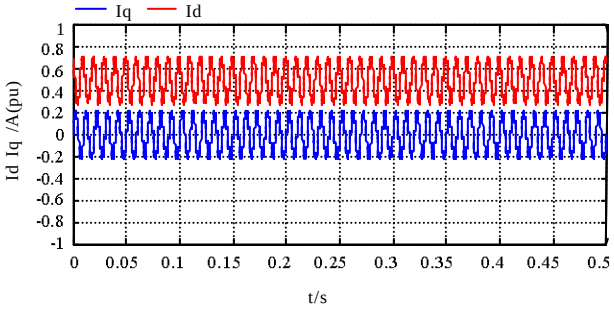

Fig. 6: The current of proportional resonant control algorithm-based inverter

inverter DC side voltage as it could control direct axis current and quadrature axis current in PWM inverter AC side currents. The curves of direct-axis current and the quadrature axis current in PWM inverter AC side currents were shown in Fig. 6. The curves of PWM inverter DC side voltage based on proportional resonant controller was shown in Fig. 7. It could be seen in Fig. 4-7 that, the PWM inverter DC side voltage had been effectively controlled and the amplitude of 2nd ripple in PWM inverter DC side voltage was effectively controlled.

DISCUSSION

The mathematical model of PWM inverter at unbalanced grid voltage was established in this study. The AC side current and DC voltage in PWM inverter was studied in depth via the symmetrical components theory. The 2nd ripple in the DC voltage and the harmonic content in the

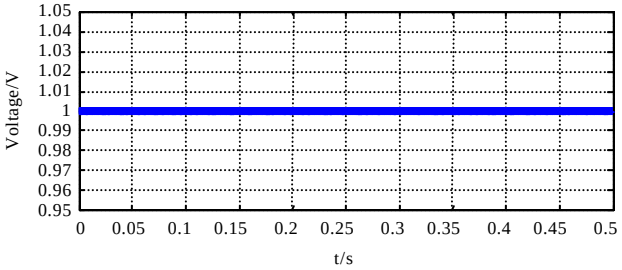

Fig. 7: The DC voltage of proportional resonant control algorithm-based inverter

AC side current could not be effectively reduced while the PWM inverter was controlled by traditional control methods. In traditional control methods, the direct axis current could be controlled but the quadrature axis current could not be effectively controlled. The direct axis current and the quadrature axis current could not effectively controlled simultaneously, so that there were the 2nd ripple in the DC voltage and plenty of harmonic content in the AC side current. The voltage or current in resonance point could be effectively controlled in proportional resonant control algorithm. The working principle of proportional resonant control strategy was analyzed and improved in this study. The proposed control strategy was applied to controlling PWM inverter at unbalanced grid voltage. Compared to the references (Martin *et al*., 2013; Wang *et al*., 2014; Karimi *et al*., 2014), it can be seen that the direct-axis component and quadrature-axis component in the AC side current of the PWM inverter could be controlled in the proposed control strategy. The 2nd ripple in the DC voltage and the harmonic content in the AC side current could be effectively reduced while the PWM inverter was controlled by the proportional resonant control algorithm. The effectiveness of the proportion of the resonant control strategy applied to controlling PWM inverter at unbalanced grid voltage was demonstrated by the simulation results in Fig. 4-7.

CONCLUSION

According to the analysis of the symmetrical components theory, the 2nd ripple emerged in the DC side voltage of PWM inverter at asymmetric grid voltages. The 2nd ripple would cause over-voltage in DC side capacitor but also would increase the substantial harmonic content in the PWM inverter AC side current. The control performance of the PWM inverter would be weakened and the grid source would be polluted. In this paper, the improved proportional resonant control strategy was applied to control PWM inverter, which could effectively reduce the 2nd ripple in PWM inverter DC side voltage. The effectiveness and the strong robustness of the proposed control strategy were verified by simulation results in this study.

ACKNOWLEDGMENTS

Project Supported by Baoji University of Arts and Sciences (GK1506). Project Supported by Baoji City Science and Technology Bureau (2013R1-2). Project Supported by National Natural Science Foundation of China (51207002).

REFERENCES

Bai, Z., H. Ma, D. Xu, B. Wu, Y. Fang and Y. Yao, 2014. Resonance damping and harmonic suppression for grid-connected current-source converter. IEEE Trans. Ind. Electron., 7: 3146-3154.

Bao, C., X. Ruan, X. Wang, W. Li, D. Pan and K. Weng, 2014. Step-by-step controller design for LCL-type grid-connected inverter with capacitor-current-feedback active-damping. IEEE Trans. Power Electron., 29: 1239-1253.

Borage, M.B., K.V. Nagesh, M.S. Bhatia and S. Tiwari, 2009. Characteristics and design of an asymmetrical duty-cycle-controlled LCL-T resonant converter. IEEE Trans. Power Electron., 24: 2268-2275.

Cetin, N.O. and A.M. Hava, 2012. Topology and PWM method dependency of high frequency leakage current characteristics of voltage source inverter driven AC motor drives. Proceedings of the IEEE Energy Conversion Congress and Exposition, September 15-20, 2012, Raleigh, North Carolina, pp: 3430-3437.

Chen, H., G. Xing, X. Zhou, M. Zhang and Y. Qu, 2013. Modified direct power control for PWM rectifier under unbalanced grid voltage conditions. Proceedings of the 32nd Chinese Control Conference, July 26-28, 2013, Xi'an, China, pp: 8874-8878.

Chu, E., M. Wu, L. Huang, X. Hou and H. Zhang, 2014. Research on a novel modulation strategy for auxiliary resonant commutated pole inverter with the smallest loss in auxiliary commutation circuits. IEEE Trans. Power Electr., 29: 1103-1117.

De Paula, H., M.L.R. Chaves, D.A. Andrade, J.L. Domingos and M.A.A. Freitas, 2005. A new strategy for differential overvoltages and common-mode currents determination in PWM induction motor drives. Proceedings of the IEEE International Conference on Electric Machines and Drives, May 15, 2005, San Antonio, TX., USA., pp: 1075-1081.

De Paula, H., D.A. De Andrade, M.L.R. Chaves, J.L. Domingos and M.A.A. De Freitas, 2008. Methodology for cable modeling and simulation for high-frequency phenomena studies in PWM motor drives. IEEE Trans. Power Electron., 23: 744-752.

Fujita, H., H. Akagi and M. Kohata, 1993. A zero-current-switching based three-phase PWM inverter having resonant circuits on AC-side. Proceedings of the Annual Meeting of Industry Applications Society, Volume 2, October 2-8, 1993, Toronto, Canada, pp: 821-826.

Hsu, J.D. and C.S. Chao, 2009. Design concepts: AC adapters for notebook computers. Power Electron. Technol., 11: 28-33.

Jung, Y.C., H.L. Liu, G.C. Cho and G.H. Cho, 1996. Soft switching space vector PWM inverter using a new quasi-parallel resonant DC link. IEEE Trans. Power Electron., 11: 503-511.

Karimi, R., E. Adib and H. Farzanehfard, 2014. Resonance based zero-voltage zero-current switching full bridge converter. IET Power Electron., 7: 1685-1690.

Malesani, L., P. Tomasin and V. Toigo, 1996. Space vector control and current harmonics in quasi-resonant soft-switching PWM conversion. IEEE Trans. Ind. Applic., 32: 269-278.

Martin, D., I. Nam, J. Siegers and E. Santi, 2013. Wide bandwidth three-phase impedance identification using existing power electronics inverter. Proceedings of the 28th Annual IEEE Applied Power Electronics Conference and Exposition, March 17-21, 2013, Long Beach, CA., USA., pp: 334-341.

Mihalache, L., 2005. A high performance DSP controller for three-phase PWM rectifiers with ultra low input current THD under unbalanced and distorted input voltage. Proceedings of the 40th IAS Annual Meeting on Industry Applications Conference, Volume 1, October 2-6, 2005, Hong Kong, pp: 138-144.

Nouri, T. and S. Ghasemzadeh, 2011. A new flexible distributed generation unit for active power generation and harmonic compensation under non-ideal source voltages condition. Proceedings of the 7th International Conference on Electrical and Electronics Engineering, December 1-4, 2011, Bursa, Turkey, pp: I-263-I-267.

Oshikata, T., Y. Saito and H. Matsuo, 2007. Analysis of PWM for three-phase PFC and suitable switching sequence for partial resonance. Proceedings of the IEEE Power Electronics Specialists Conference, June 17-21, 2007, Orlando, FL., USA., pp: 1304-1308.

Pan, D., X. Ruan, W. Li and X. Wang, 2014. Capacitor-current-feedback active damping with reduced computation delay for improving robustness of LCL-type grid-connected inverter. IEEE Trans. Power Electron., 7: 3414-3427.

Pokryszko-Dragan, A., J. Bladowska, A. Zimny, K. Slotwinski and M. Zagrajek *et al*., 2014. Magnetic resonance spectroscopy findings as related to fatigue and cognitive performance in multiple sclerosis patients with mild disability. J. Neurol. Sci., 339: 35-40.

Qu, K.Q. and J.B. Zhao, 2014. Novel three-phase pwm voltage-fed rectifier with an auxiliary resonant commutated pole link. J. Power Electron., 4: 678-686.

Russi, J.L., V.F. Montagner, M.L.S. Martins and H.L. Hey, 2013. A simple approach to detect ZVT and determine its time of occurrence for PWM converters. IEEE Trans. Ind. Electron., 60: 2576-2585.

Shiraishi, K., K. Imamura, Y. Fujii, M. Nakamura, T. Ahmed, M. Nakaoka and H.W. Lee, 2004. Active auxiliary resonant snubber-assisted soft-switching PWM inverter with optimum gate pulse pattern sequences and its PV-system application. Proceedings of the 35th Annual Conference on Power Electronics Specialists, Volume 5, June 20-25, 2004, Aachen, Germany, pp: 3971-3977.

Soltanzadeh, K., M. Dehghani and H. Khalilian, 2014. Analysis, design and implementation of an improved ZVZCS-PWM forward converter. J. Electr. Eng. Technol., 9: 197-204.

Suh, Y. and T.A. Lipo, 2004. A control scheme of improved transient response for PWM AC/DC converter under generalized unbalanced operating conditions. Proceedings of the 35th Annual Conference on Power Electronics Specialists, Volume 1, June 20-25, 2004, Aachen, Germany, pp: 189-195.

Wang, S., L.C. Tan, Y.H. Li, P. Wang, H.T. Ren and P.X. Song, 2014. Current tracking strategies of cascade STATCOM under two-phase coordinate system. Electric Mach. Control, 1: 19-25.

Xu, J., S. Xie and T. Tang, 2014. Active damping-based control for grid-connected LCL-filtered inverter with injected grid current feedback only. IEEE Trans. Ind. Electron., 9: 4746-4758.

Xu, Z., L. Luo, Z. Zhang and Y. Li, 2013. An improved three-phase V/v traction transformer and its compensation method. Proc. CSEE, 30: 128-135.

Yang, H., H. Lin, Y. Lv, Y. Luo and X. Wang, 2013. A multi-resonant PR inner current controller design for reversible PWM rectifier. Proceedings of the 28th Annual IEEE Applied Power Electronics Conference and Exposition, March 17-21, 2013, Long Beach, CA., USA., pp: 316-320.

Zeng, Z., J.Q. Yang, S.L. Chen and J. Huang, 2014. Fast-transient repetitive control strategy for a three-phase LCL filter-based shunt active power filter. J. Power Electron., 14: 392-401.

Zhan, M.H., M.C. Wong and Y.D. Han, 2005. Quasi-resonant dc link control of 3-dimensional hysteresis current PWM technique in 3-phase 4-wired power quality compensator. Proceedings of the IEEE/PES Transmission and Distribution Conference and Exhibition: Asia and Pacific, August 14-18, 2005 Dalian, China, pp: 1-6.